Journal of Alloys and Compounds 905 (2022) 164022

Contents lists available at ScienceDirect

Journal of Alloys and Compounds

journal homepage: www.elsevier.com/locate/jalcom

New double nonlinear-optical borate $Rb_3SmB_6O_{12}$: Synthesis, structure and spectroscopic properties

Victor Atuchin[a,b,c,d,*], Alexey Subanakov[e], Aleksandr Aleksandrovsky[f,g], Bair Bazarov[e], Jibzema Bazarova[e], Alexander Krylov[h], Maxim Molokeev[i,j,k], Aleksandr Oreshonkov[h,l], Alexey Pugachev[m]

[a] Laboratory of Optical Materials and Structures, Institute of Semiconductor Physics, SB RAS, Novosibirsk 630090, Russia
[b] Research and Development Department, Kemerovo State University, Kemerovo 650000, Russia
[c] Department of Applied Physics, Novosibirsk State University, Novosibirsk 630090, Russia
[d] Department of Industrial Machinery Design, Novosibirsk State Technical University, Novosibirsk 630073, Russia
[e] Laboratory of Oxide Systems, Baikal Institute of Nature Management, SB RAS, Ulan-Ude 670047, Russia
[f] Laboratory of Coherent Optics, Kirensky Institute of Physics Federal Research Center KSC SB RAS, Krasnoyarsk 660036, Russia
[g] Department of Photonics and Laser Technology, Siberian Federal University, Krasnoyarsk 660041, Russia
[h] Laboratory of Molecular Spectroscopy, Kirensky Institute of Physics Federal Research Center KSC SB RAS, Krasnoyarsk 660036, Russia
[i] Laboratory of Crystal Physics, Kirensky Institute of Physics, Federal Research Center KSC SB RAS, Krasnoyarsk 660036, Russia
[j] Siberian Federal University, Krasnoyarsk 660041, Russia
[k] Department of Physics, Far Eastern State Transport University, Khabarovsk 680021, Russia
[l] School of Engineering and Construction, Siberian Federal University, 660041 Krasnoyarsk, Russia
[m] Laboratory of Condensed Matter Spectroscopy, Institute of Automation and Electrometry, Novosibirsk 630090, Russia

ARTICLE INFO

Article history:
Received 29 December 2021
Received in revised form 21 January 2022
Accepted 27 January 2022
Available online 1 February 2022

Keywords:
Borate
Crystal structure
Raman
Photoluminescence

ABSTRACT

New noncentrosymmetric alkali rare-earth double borate $Rb_3SmB_6O_{12}$ was found in the ternary system Rb_2O–Sm_2O_3–B_2O_3. The $Rb_3SmB_6O_{12}$ powder was prepared by the solid state reaction method at 750 °C for 40 h and the crystal structure was obtained by the Rietveld method. $Rb_3SmB_6O_{12}$ crystallized in space group *R*32 with unit cell parameters a = 13.4874 (3) and c = 30.9398 (6) Å, V = 4874.2 (2) Å^3, Z = 15. In the three-dimensional framework structure of $Rb_3SmB_6O_{12}$, each $[B_5O_{10}]^{5-}$ group is linked to four different Sm-O polyhedra and, likewise, each Sm-O polyhedron is connected to four neighboring $[B_5O_{10}]^{5-}$ groups. The Sm-O polyhedra are formed by the face-sharing linked SmO_6 octahedra. Rb^+ cations are located in large cavities of the framework structure. From the thermal stability measurements, the incongruent melting of $Rb_3SmB_6O_{12}$ is observed at 1104 K with as high melting enthalpy as H_m = –161.5 J/g. The nonlinear optical response of $Rb_3SmB_6O_{12}$ tested via SHG is estimated to be similar to that of $K_3YB_6O_{12}$. The Raman spectrum of $Rb_3SmB_6O_{12}$ is mainly governed by the vibrations of BO_4 and BO_3 borate groups observed over the wavenumber range of 287–1550 cm^{-1}. The spectral bands below 270 cm^{-1} were attributed to rotational, translational and mixed vibrations of $Rb_3SmB_6O_{12}$ structural units. The luminescence spectrum of Sm^{3+} ions in the specific local environment of the $Rb_3SmB_6O_{12}$ crystal lattice shows the ability to control the individual band intensity ratio originating from $^4G_{5/2}$ level.

1. Introduction

Borate crystals have their rich crystal chemistry that opens a possibility for the construction of specified materials with different combinations of physicochemical properties [1–6]. In particular, borate crystals are valuable as optical materials because of appropriate chemical and mechanical stabilities, a wide transparency range and high optical damage threshold [1,6–14]. Accordingly, the crystal growth technology was developed for selected borate materials to reach the large-sized low-defect single crystals appropriate for the application in high-power laser systems [15–20]. Many known and new borate crystals have been investigated in recent years in the search for materials with promising nonlinear optical, piezoelectric, thermophysical and spectroscopic characteristics [20–36]. Among borate compounds, crystals containing rare earth

* Correspondence to: Institute of Semiconductor Physics, Novosibirsk 630090, Russia.
E-mail address: atuchin@isp.nsc.ru (V. Atuchin).

https://doi.org/10.1016/j.jallcom.2022.164022
0925-8388/

ions are of particular interest because they can be used as hosts in laser and photonic technologies.

The double borates of general formula $A_3LnB_6O_{12}$ (A = K or Rb, Ln = Y or rare earths) have attracted considerable attention because of their curious structural and nonlinear optical properties, which make them promising for various applications [28,29,37–43]. It should be pointed that $A_3LnB_6O_{12}$ compounds are known only for A = K or Rb and the existence of this structure type for other alkaline metals and Tl is unclear. $A_3LnB_6O_{12}$ compounds crystallize in the noncentrosymmetric trigonal space group *R*32 and are characterized by a short UV cutoff edge, appropriate nonlinear optical properties and high thermal stability [28,29,38,40]. A centimeter-sized $K_3YB_6O_{12}$ crystal was successfully grown by the top-seeded solution growth method using a $K_2O–B_2O_3–KBF_4$ flux [37]. Later, a series of $K_3LnB_6O_{12}$-based phosphors was synthesized and their structural and photoluminescence characteristics were evaluated [39,41–48]. Today, it turns out that $K_3LnB_6O_{12}$ compounds are formed for a wide composition range, at least for Ln = Y or Lu-Eu [46,49]. As to Rb-containing borates, the information is evidently scarce and only four compositions, namely, $Rb_3LnB_6O_{12}$ Ln = Y, Ho, Eu and Nd, were tested in experiments [28,29,38,40]. The present study is aimed at the synthesis of double borate $Rb_3SmB_6O_{12}$ and the exploration of its structural, thermal and spectroscopic characteristics. In the structure, the photoluminescence parameters of Sm^{3+} ion can be determined under the precise control of their crystallographic environment, and it opens a possibility for the creation of efficient phosphors, emitting in the red-orange range, on the base of related hosts, including $Rb_3YB_6O_{12}$. The synthesis of $Rb_3SmB_6O_{12}$ was carried out by the solid state reaction method. The structural, thermal and spectroscopic characteristics of the compound were determined by conventional experimental techniques.

2. Methods and materials

The $Rb_3SmB_6O_{12}$ compound was prepared by the solid state reactions using high-purity starting reagents: Rb_2CO_3 (99.8%, Sigma Aldrich Ltd.), Sm_2O_3 (99.9%, Red Chemist, Ltd., Russia), and H_3BO_3 (99.5%, Sigma Aldrich Ltd.). Before weighing, Rb_2CO_3 and Sm_2O_3 were preheated at 850 °C for 8 h to remove any absorbed water. In the batch preparation, according to the stoichiometric composition, the reagents were weighed on an analytical balance with the accuracy of 0.5 mg. The mixtures of Rb_2CO_3, Sm_2O_3 and H_3BO_3 at molar ratio 3:1:12 were thoroughly ground in an agate mortar, slowly heated to 500 °C and held for 5 h in the air atmosphere. After that, the samples were then reground and annealed at 600 °C for 5 h with intermediate grindings and, finally, at 750 °C for 40 h until the equilibrium was reached. The equilibrium was specified only when two successive heat treatments resulted in identical X-ray diffraction patterns. Temperatures were measured with a Pt–PtRh thermocouple. The temperature was controlled to be within ± 2 °C with an OMRON controller. The photo of the synthesized powder sample is shown in Fig. 1. The powder was flowy and uniform. The light-orange tint was observed for the samples and it is a characteristic color of Sm^{3+}-containing oxides [50–52].

The powder diffraction data of $Rb_3SmB_6O_{12}$ for Rietveld analysis were collected at room temperature with a Bruker D8 ADVANCE powder diffractometer (Cu-Kα radiation) and linear VANTEC detector. The step size of 2θ was 0.021°, and the counting time was 30 s per step. Rietveld refinement was performed by using TOPAS 4.2 [53]. Almost all peaks were indexed by the trigonal cell (space group *R*32) with the cell parameters close to $Rb_3EuB_6O_{12}$ [40]. Therefore, this crystal structure was taken as a starting model for Rietveld refinement, and only the Eu ion was replaced by the Sm ion. The refinement was stable and gave low *R*-factors (Table 1, Fig. 2). The coordinates of atoms and the main bond lengths in the $Rb_3SmB_6O_{12}$ structure are given in Tables S1 and S2, respectively. The

Fig. 1. Photo of as-synthesized $Rb_3SmB_6O_{12}$ powder sample.

Table 1
Main parameters of processing and refinement of the $Rb_3SmB_6O_{12}$ sample.

Compound	$Rb_3SmB_6O_{12}$
Sp.Gr.	*R*32
a, Å	13.4874 (3)
c, Å	30.9398 (6)
V, Å^3	4874.2 (2)
Z	15
2*θ*-interval, º	10–100
R_{wp}, %	1.67
R_p, %	1.15
R_{exp}, %	0.62
χ^2	2.69
R_B, %	1.07

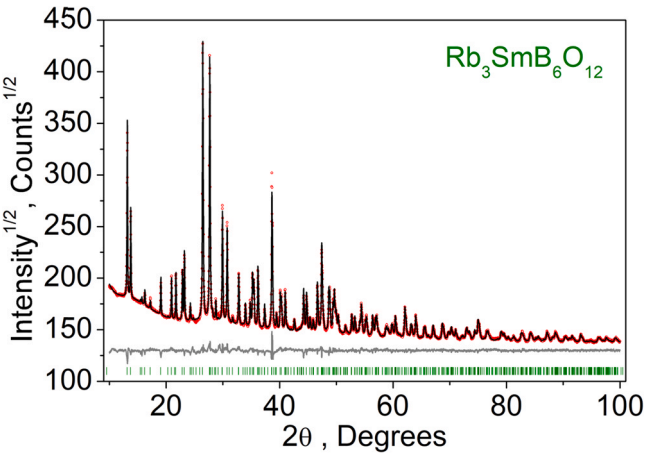

Fig. 2. Difference Rietveld plots of $Rb_3SmB_6O_{12}$.

crystallographic data are deposited in Cambridge Crystallographic Data Centre (CCDC # 2131404). The data can be downloaded from the site (www.ccdc.cam.ac.uk/data_request/cif).

The SHG response was measured in the back-scattering geometry by means of the modified Kurtz–Perry powder method [54]. The sample SHG was excited by the ns pulsed radiation of a Nd:YAG laser (STA-01–7, Standa) working at λ = 1064 nm with the 100 mW mean power. The detailed description of the experimental set up and the measurement conditions can be found elsewhere [55]. Crystalline quartz was used as a reference, and the relation $SHG(Rb_3SmB_6O_{12}) = 6.5 \times SHG(\alpha\text{-}SiO_2)$ verifies the selection of noncentrosymmetric space group for $Rb_3SmB_6O_{12}$.

Differential scanning calorimetric (DSC) and thermogravimetric (TG) measurements were performed on an STA 449 F1 Jupiter thermoanalyzer (NETZSCH) over the temperature range of 30–1150 °C in the argon flow. Pt crucibles were used as vessels. Pt-PtRh thermocouples were used for the measurement. The temperature measurement precision was ± 1 °C. The heating and cooling rates were 10 °C/min.

The experimental Raman spectra of $Rb_3SmB_6O_{12}$ compound were acquired using a triple monochromator Horiba Jobin Yvon T64000 Raman spectrometer operating in the subtractive mode in the backscattering geometry and were detected by a liquid nitrogen-cooled CCD cooled to 140 K. The spectral resolution for the recorded Stokes side Raman spectra was about 2 cm^{-1}, and the pixel coverage was 0.3 cm^{-1}. The single-mode radiation λ = 514.5 nm from the Spectra-Physics Stabilite 2014 Ar^+ laser was used as an excitation light source, the power on the sample being 3 mW.

Photoluminescence measurements were performed with the help of Horiba Jobin Yvon T64000 spectrophotometer using laser excitation at several selected generation lines from the Spectra Physics Stabilite 2017 Ar ion laser. The T64000 spectrophotometer is featured by a very high signal to noise ration that enabled obtaining high quality luminescent spectra from the sample with a high luminescent ion concentration.

3. Results and discussions

3.1. Crystal structure

The crystal structure of $Rb_3SmB_6O_{12}$ is shown in Fig. 3. The $Rb_3SmB_6O_{12}$ structure contains a three-dimensional framework composed of $[B_5O_{10}]^{5-}$ groups bridged by Sm-O polyhedra (Fig. 3). The $[B_5O_{10}]^{5-}$group consists of one BO_4 tetrahedron and four BO_3 triangles that form double B-O rings via the common tetrahedron. All the B-O rings in this structure can be divided into two groups, with one group approximately parallel and the other - perpendicular to the *c* axis. Each $[B_5O_{10}]^{5-}$ group is bound to four different Sm-O polyhedra and, likewise, each Sm-O polyhedron is bound to four neighboring $[B_5O_{10}]^{5-}$ groups. The Sm-O polyhedra are formed by the face-sharing linked SmO_6 octahedra. Rb^+ cations are located in large cavities of the framework structure (Fig. 3). Checking crystal structure for the presence of missed symmetry elements revealed the presence of possible pseudotranslation *c*/2. However, there is the Rb ion which breaks this translation, as seen in Fig. 3, and only $[B_5O_{10}]^{5-}$ structural motifs are arranged with pseudotranslation. It should be noted that, under some conditions, the Rb/Sm disordering is probable and can lead to the appearance of this new *c*/2 translation and phase transition.

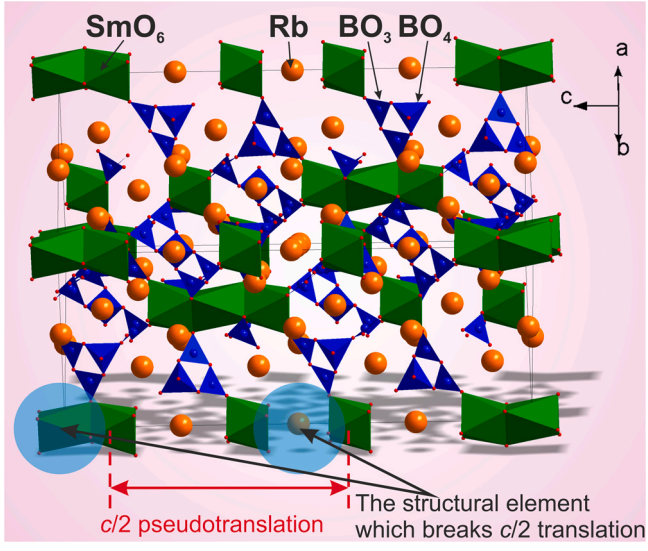

Fig. 3. Crystal structure of $Rb_3SmB_6O_{12}$. The unit cell is outlined. Lone atoms, except Rb, are omitted for clarity.

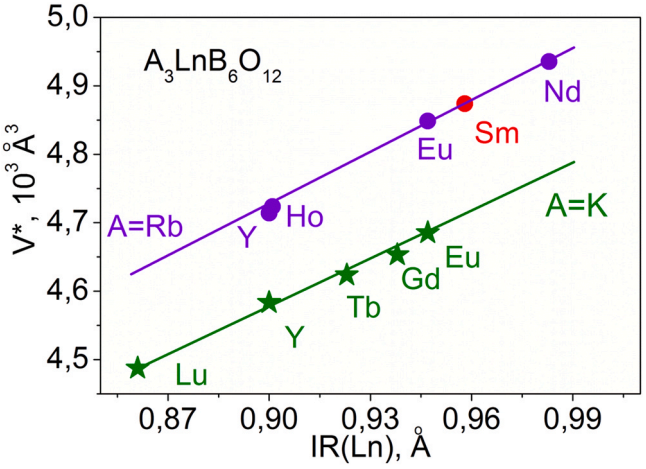

Fig. 4. Cell volume dependence *per* ion radii of Ln and A elements in the known $A_3LnB_6O_{12}$ compounds with A = Rb and K. The V* values are calculated from cell volume V by formula V* = V× 15/Z, where Z is the number of formula units in the unit cell.

The unit cell volume (for Z = 15) dependence on the effective radius of Ln^{3+} ion in $A_3LnB_6O_{12}$ compounds is shown in Fig. 4. The structural parameters of the known $A_3LnB_6O_{12}$ compounds are presented in Table 2. The effective Ln^{3+} ion radii for coordination number 6 were considered [57]. As it is seen in Fig. 4, the dependences for K and Rb can be well fitted by linear functions V* = 2211.05 ×IR(Ln) + 2586.04 and V* = 2656.56 ×IR(Ln) + 2327.82, respectively. In the $A_3LnB_6O_{12}$ family, the trigonal structure is persisted for a wide range of Ln elements. In the $K_3LnB_6O_{12}$ crystals, the lowest possible unit cell volume value is reached in $K_3LuB_6O_{12}$, but the upper limit for the existence of this structure is unclear today. The $Rb_3LnB_6O_{12}$ crystals are known for bigger ions Sm^{3+} and Nd^{3+}, but the upper and lower limits of the subfamily remain unclear.

Table 2
Known compounds $A_3LnB_6O_{12}$ and their cell parameters.

Chemical composition	Space group, Z	Cell parameters, Å	Cell volume, $Å^3$	Reference
$K_3LuB_6O_{12}$	*R*32, 7.5	*a* = 13.1549 (8), *c* = 14.9713 (9)	2243.7(3)	[46]
$K_3YB_6O_{12}$	*R*32, 15	*a* = 13.2202 (19), *c* = 30.281 (6)	4583.29(1)	[37]
$K_3TbB_6O_{12}$	*R*32, 7.5	*a* = 13.2310 (12), *c* = 15.2490 (6)	2311.8(4)	[56]
$K_3GdB_6O_{12}$	*R*32, 7.5	*a* = 13.2490 (9), *c* = 15.3038 (10)	2326.5(4)	[47]
$K_3EuB_6O_{12}$	*R*32, 7.5	*a* = 13.2610 (17), *c* = 15.3822 (19)	2342.6(7)	[49]
$Rb_3EuB_6O_{12}$	*R*32, 15	*a* = 13.4732 (2), *c* = 30.8424 (6)	4848.6(2)	[40]
$Rb_3SmB_6O_{12}$	*R*32, 15	*a* = 13.4874 (3), *c* = 30.9398 (6)	4874.2(2)	This work
$Rb_3NdB_6O_{12}$	*R*32, 15	*a* = 13.5236 (4), *c* = 31.1617 (10)	4935.6(3)	[38]
$Rb_3YB_6O_{12}$	*R*32, 7.5	*a* = 13.3894 (3), *c* = 15.2031 (7)	2357.1(3)	[31]
$Rb_3HoB_6O_{12}$	*R*32, 15	*a* = 13.4078 (2), *c* = 30.3398 (4)	4723.45(12)	[30]

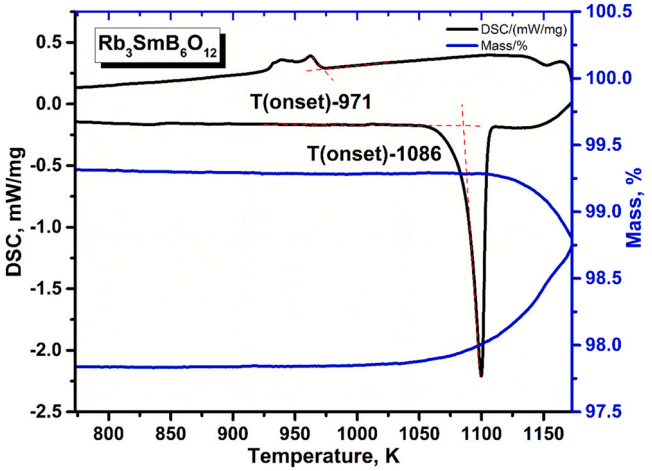

Fig. 5. . DSC/TG curves recorded for $Rb_3SmB_6O_{12}$.

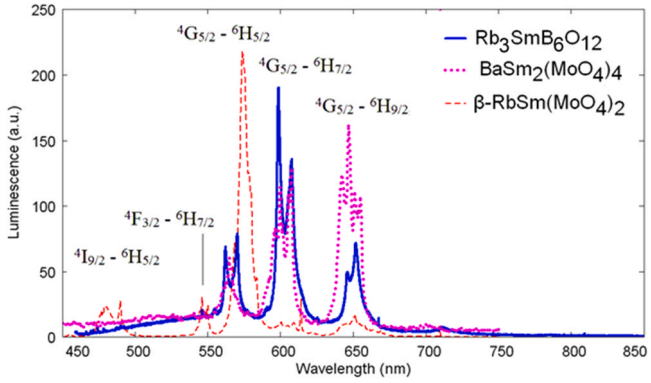

Fig. 6. Emission spectrum of $Rb_3SmB_6O_{12}$ excited at 457.9 nm in comparison with those of Sm^{3+}-containing molybdates excited at 355 nm.

3.2. Thermochemical properties

The results of the simultaneous (TG/DSC) thermal analysis of $Rb_3SmB_6O_{12}$ from 378 to 1173 K are shown in Fig. 5. The DSC heating curve clearly indicates the endothermic effect corresponding to the melting of the double borate $Rb_3SmB_6O_{12}$ at ($T_{melting}$ (peak) = 1104 K, $T_{melting}$ (onset) = 1086 K, ΔH = −161.5 J/g). The twinned exothermal effect (T (onset) = 971 K, ΔH = 17.6 J/g) at the DSC cooling curve related to the crystallization of the residues appeared after the melt decomposition of $Rb_3SmB_6O_{12}$. The incongruent melting of $Rb_3SmB_6O_{12}$ is additionally confirmed by the XRD patterns of the residual keck extracted after cooling (Fig. S1). Among the crystalline residues, such compounds as $Rb_2(B_4O_5OH)_4(H_2O)_{3.6}$ (PDF 00–051–0233) [58], $SmBO_3$ (PDF 00–013–0489) [59], B_2O_3 (PDF 73–1550) [60] were revealed. Besides the crystalline compounds, the amorphous component is significant. In our opinion, at high temperatures, $Rb_3SmB_6O_{12}$ is decomposed to $SmBO_3$ and $Rb_2B_4O_7$. In the cooling process and at room temperature, $Rb_2B_4O_7$ immediately interacts with the air moisture and it results in the formation of $Rb_2(B_4O_5OH)_4(H_2O)_{3.6}$. During the heating and cooling, the TG curve is very clear and there is no weight loss. This indicates complete absence of volatile impurities or components.

The thermal characteristics of the presently known double borates $A_3LnB_6O_{12}$ (A = K, Ln = Eu-Tb, Lu and Y; A = Rb, Ln = Nd, Sm, Eu, Ho and Y) are summarized in Table 3. The solid-state reaction technique was applied in the preparation of all compounds, except for $Rb_3HoB_6O_{12}$ which was manufactured by the sol-gel method [30]. Unfortunately, the melting investigation of K-containing borates was carried out only for $K_3YB_6O_{12}$ [37]. Phase transitions were observed for $Rb_3LnB_6O_{12}$, Ln = Nd and Ho. Some trend can be seen for the melting temperatures of Rb-containing compounds. The melting temperatures of $Rb_3SmB_6O_{12}$ and $Rb_3EuB_6O_{12}$ are noticeably higher than those of $Rb_3NdB_6O_{12}$ and $Rb_3HoB_6O_{12}$. It is interesting that the phase formation enthalpy values are also higher for $Rb_3SmB_6O_{12}$ and $Rb_3EuB_6O_{12}$. These relations may be an indication of the increased $Rb_3LnB_6O_{12}$ structure stability for middle Ln elements. To verify the assumption, for comparison, it could be valuable to observe the melting temperatures and phase formation enthalpies of the $K_3LnB_6O_{12}$ borates.

3.3. Luminescence properties

Fig. 6 depicts the luminescence spectrum of $Rb_3SmB_6O_{12}$ excited at 457.9 nm in comparison with the spectra of β-$RbSm(MoO_4)_2$ [50] and $BaSm_2(MoO_4)_4$ [51]. The luminescence spectrum of $Rb_3SmB_6O_{12}$ contains noticeable broad band forming the background for the luminescent bands of Sm^{3+} ion. This background protrudes from the 460–750 nm peaking approximately at 570 nm. The luminescent contribution of Sm^{3+} in $Rb_3SmB_6O_{12}$ is somehow similar to that in $BaSm_2(MoO_4)_4$ and strongly differs from that in β-$RbSm(MoO4)_2$. The latter must be ascribed to different local symmetry of the Sm^{3+} ions in $Rb_3SmB_6O_{12}$ and β-$RbSm(MoO4)_2$. Specifically, the $^4G_{5/2}$ – $^6H_{5/2}$ band experiences a strong intensity redistribution of the transitions between individual crystal field split sublevels with respect to β-$RbSm(MoO4)_2$, so, this band peak shifts from 574 to 570 nm. $^4G_{5/2}$ – $^6H_{7/2}$ and $^4G_{5/2}$ – $^6H_{9/2}$ bands experience smaller distortion. However, their relative intensity is greatly increased with respect to those in β-$RbSm(MoO4)_2$. The $^4F_{3/2}$ – $^6H_{7/2}$ transition is observable as a very small peak hardly distinguishable over the background, while the $^4I_{9/2}$ – $^6H_{5/2}$ band is completely undistinguishable, and only Raman spectral features are observable in the spectral region it might occupy. The differences of the luminescence spectra between $Rb_3SmB_6O_{12}$ and another reference crystal, $BaSm_2(MoO_4)_4$ are less pronounced, though one may note that the maximum band in the borate under study is the $^4G_{5/2}$ – $^6H_{7/2}$ one, while in $BaSm_2(MoO_4)_4$ the $^4G_{5/2}$ – $^6H_{9/2}$ one prevails. Sm ions in trigonal lattice of $Rb_3SmB_6O_{12}$ occupy three inequivalent positions

Table 3
Thermal parameters of compounds $A_3LnB_6O_{12}$.

Compound	Ion radii of Ln^{3+}, Å	Synthesis: Temperature, K / Time, h	Phase transition / Melting point, K	Enthalpy, J/g	Reference
$K_3EuB_6O_{12}$	0.947	1023/24	–	–	[49]
$K_3GdB_6O_{12}$	0.938	1033/20	–	–	[47]
$K_3TbB_6O_{12}$	0.923	1023/72	–	–	[56]
$K_3YB_6O_{12}$	0.900	973/120	-/1214	–	[37]
$K_3LuB_6O_{12}$	0.861	1023/48	–	–	[46]
$Rb_3NdB_6O_{12}$	0.983	973–1023/24–72	936/1070	−122.4	[38]
$Rb_3SmB_6O_{12}$	0.958	1023/40	-/1104	−161.5	This work
$Rb_3EuB_6O_{12}$	0.947	973–1023/24–72	-/1101	−160.6	[40]
$Rb_3HoB_6O_{12}$	0.901	facile sol-gel method and calcined at 1023/5	988/1091	−120.7	[30]
$Rb_3YB_6O_{12}$	0.900	973/48	-/1094	–	[31]

with local symmetry C_3 (two sites) and D_3 (third site) while, e.g., in β-$RbSm(MoO_4)_2$ Sm^{3+} ions occupy a single site with the local symmetry C_2. Distribution of bands in $Rb_3SmB_6O_{12}$ is the average over that from three different sites and, therefore, this distribution is somehow intermediate one between two reference crystals.

The $Rb_3SmB_6O_{12}$ excitation at another wavelength, 514.5 nm, leads to the luminescence spectrum of Sm^{3+} ions that is generally very close to that excited at 457.9 nm. Both laser wavelengths used to excite the $Rb_3SmB_6O_{12}$ luminescence are out of evident resonance with Sm^{3+} ion transitions from the ground state. Then we must assume that they fall into a weak and broad absorption band of some point defects of the crystal structure, e.g. anion vacancies or something else. These vacancies concentration is expected to be rather small in view of a good quality of the XRD pattern. Excitation of these vacancies leads to the energy transfer to $^4I_{9/2}$ (in case of the 457.9 nm excitation wavelength) or to $^4F_{3/2}$ (in case of the 514.5 nm excitation wavelength) with the subsequent radiativeless relaxation to $^4G_{5/2}$ and the luminescence from this state. Assuming that non-resonant Raman cross section is the same for both excitation wavelengths and calibrating the laser power by the Raman lines intensity, we deduce that the Sm^{3+} luminescence excited at 457.9 nm is 32.7 times higher than that excited at 514.5 nm. This value reflects the ratio of absorption cross sections of the defects multiplied by energy transfer probability for every excitation wavelength. It is interesting to note that the β-RbSm(MoO4)$_2$ reference crystal spectrum contains no background invoking that the point defect concentration in the reference crystal is much smaller than that in the borate under study.

3.4. Vibrational properties

The Raman spectrum of $Rb_3SmB_6O_{12}$ measured at room temperature is shown in Fig. 7. The group theory analysis predicts 220 vibrational modes with the following irreducible representations $\Gamma_{vibr} = 53A_1 + 57A_2 + 110E$, where the A_1 and A_2 modes correspond to non-degenerate modes, while the E modes are double-degenerate. Here, the acoustic modes are $A_2 + E$, while the Raman- and infrared-active modes are as follows: $\Gamma_{Raman} = 53A_1 + 109E$, $\Gamma_{Infrared} = 56A_2 + 109E$. The contribution of particular ions to vibrational spectra [61] can be found in Table 4. At the same time, as it was shown above, the crystal structure of $Rb_3SmB_6O_{12}$ contains $[B_5O_{10}]^{5-}$ units consisting of the BO_4 tetrahedron and BO_3 triangles. The Raman spectrum range from 1180 to 1550 cm^{-1} is related to the ν_3-like antisymmetric

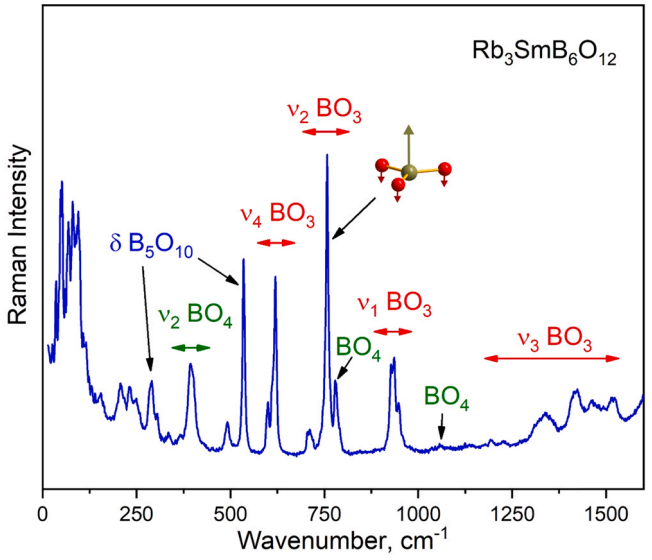

Fig. 7. Raman spectrum of $Rb_3SmB_6O_{12}$ powder.

Table 4
Wyckoff positions of ions and corresponding irreducible representations of vibrational modes in structure of $Rb_3SmB_6O_{12}$.

Ion	Wyckoff notation	Irreducible representations
Rb3, B1–5, O1–10	18 f	$3A_1 + 3A_2 + 6E$
Sm1–2, Rb4	6c	$A_1 + A_2 + 2E$
Sm3	3a	$A_2 + E$
Rb1	9e	$A_1 + 2A_2 + 3E$
Rb2	9d	$A_1 + 2A_2 + 3E$
Rb5	3b	A2 + E

stretching vibrations of BO_3 triangles [62]. The BO_3 symmetric stretching is located between 910 and 956 cm^{-1} [40]. The out-of-plane bending of BO_3 groups located in the range of 690–810 cm^{-1} and the graphical presentation of the vibration related to the strongest Raman line are shown in Fig. 7. The in-plane BO_3 vibrations appeared in the spectrum as the lines in the wavenumber range from 585 to 635 cm^{-1} [63]. The weak bands around 1600 cm^{-1} are related to the O-B-O antisymmetric stretching in the BO_4 unit of the $[B_5O_{10}]^{5-}$ pentaborate group. The Raman peak observed at 780 cm^{-1} is attributed to the B-O stretching vibrations in BO_4 [64]. Due to the fact that BO_4 and BO_3 are bound to each other inside the pentaborate molecule, the spectral band at 536 cm^{-1} can be described as the bending of B_5O_{10} [64]. The bending-like ν_2 vibrations of BO_4 tetrahedra are located in the range of 365–420 cm^{-1} [65]. The peak at 287 cm^{-1} is related to the bending vibrations of the B_5O_{10} group [64]. The spectral bands below 270 cm^{-1} should be attributed to the rotational, translational and mixed vibrations of $Rb_3SmB_6O_{12}$ structural units [38]. Thus, the Raman spectrum of $Rb_3SmB_6O_{12}$ is mainly governed by the vibrations of BO_4 and BO_3 borate groups.

4. Conclusions

In the present study, a new noncentrosymmetric borate $Rb_3SmB_6O_{12}$ was synthesized and its basic properties were evaluated. The discovery of this compound increased the number of the known crystals of double trigonal borates $A_3LnB_6O_{12}$ (A = K or Rb, Ln = Y or rare earths), and, accordingly, some general trends in this family become clearer. As it is seen, high nonlinear optical property level cannot be reached in $A_3LnB_6O_{12}$ because of the specific orientation of BO_3 and BO_4 borate groups in this structure. Besides, the growth of big crystals by the industrial Czochralski method seems to be impossible, at least, for many compositions because of the incongruent melting commonly observed in the borates from the $A_3LnB_6O_{12}$ family. These two factors greatly complicate the application of these borates in frequency conversion systems and the laser technology. However, for several borates from the $A_3LnB_6O_{12}$ family, including $Rb_3SmB_6O_{12}$, a good thermal stability was observed, and this is a promising factor for the creation of efficient phosphor materials. The stability of the matrix structure for a range of Ln elements opens the way for high doping levels in the solid solutions on the base of $A_3LnB_6O_{12}$ without structural defects generation, and it is a promising feature for low optical losses in the phosphor systems.

The luminescence spectrum of Sm^{3+} ion in the specific local environment of the $Rb_3SmB_6O_{12}$ crystal lattice shows the luminescent band intensities distribution that is an intermediate one between such reference molybdate crystals like $BaSm_2(MoO_4)_4$ and β-$RbSm(MoO4)_2$. Specifically, β-$RbSm(MoO4)_2$ shows the domination of orange band $^4G_{5/2} - {}^6H_{5/2}$, while $BaSm_2(MoO_4)_4$ - domination of deep-red $^4G_{5/2} - {}^6H_{9/2}$ band. The crystal under study demonstrates an intermediate case, e. g. the domination of mild-red $^4G_{5/2} - {}^6H_{7/2}$ band.

To determine the boundaries of the $A_3LnB_6O_{12}$ family, the existence of trigonal borates should be tested for different A and Ln elements. As to A^+ ions, first, such ions as Na^+, Cs^+ and Tl^+ should be

considered. Besides pure compounds, wide-ranged solid solutions could be investigated, and that open a possibility for tuning the emission properties of rare earth ions.

CRediT authorship contribution statement

Victor Atuchin: Conceptualization; Writing – review & editing. **Alexey Subanakov:** Conceptualization; Data curation; Writing – original draft. **Aleksandr Aleksandrovsky:** Formal analysis; Writing – original draft. **Bair Bazarov:** Methodology. **Jibzema Bazarova:** Supervision. **Alexander Krylov:** Data curation. **Maxim Molokeev:** Data curation; Formal analysis, **Aleksandr Oreshonkov:** Formal analysis. **Alexey Pugachev:** Data curation.

Declaration of Competing Interest

The authors declare that they have no known competing financial interests or personal relationships that could have appeared to influence the work reported in this paper.

Acknowledgments

This work was supported by the Ministry of Science and Higher Education of Russia (project 0273-2021-0008) and the Russian Science Foundation (project 21-19-00046, in part of conceptualization). Also, this study was partly funded by RFBR (project No. 20–33-90188a) and State assignment Basic Project of IA&E SB RAS No 121032400052-6. The X-ray powder diffraction and thermal analysis were obtained using the equipment of the Collective Use Center BINM SB RAS. The Raman and luminescence experiments were performed in the Krasnoyarsk Regional Center of Research Equipment of Federal Research Center «Krasnoyarsk Science Center SB RAS.

Appendix A. Supporting information

Supplementary data associated with this article can be found in the online version at doi:10.1016/j.jallcom.2022.164022.

References

[1] T. Thao Tran, Hongwei Yu, James M. Rondinelli, Kenneth R. Poeppelmeier, P. Shiv, Halasyamani, Deep ultraviolet nonlinear optical materials, Chem. Mater. 28 (2016) 5238–5258.
[2] Yaoguo Shen, Sangen Zhao, Junhua Luo, The role of cations in second-order nonlinear materials based on π-cojugated $[BO_3]^{3-}$ groups, Coord. Chem. Rev. 366 (2018) 1–28.
[3] Yanna Chen, Min Zhang, Miriding Mutailipu, Kenneth R. Poeppelmeier, Shilie Pan, Research and development of zincoborates: Crystal growth, structural chemistry and physicochemical properties, Molecules 24 (2019) 2763.
[4] Nikolay I. Leonyuk, Victor V. Maltsev, Elena A. Volkova, Crystal chemistry of high- temperature borates, Molecules 25 (2020) 2450.
[5] Si-Han Yang, Huaiguo Xue, Sheng-Ping Guo, Borates as promising electrode materials for rechargeable batteries, Coord. Chem. Rev. 427 (2021) 213551.
[6] Miriding Mutailipu, Kenneth R. Poeppelmeier, Shilie Pan, Borates: A rich source for optical materials, Chem. Rev. 121 (3) (2021) 1130–1202.
[7] Takatomo Sasaki, Yusuke Mori, Masashi Yoshimura, Yoke Khin Yap, Tomosumi Kamimura, Recent development of nonlinear optical borate crystals: key materials for generation of visible and UV light, Mater. Sci. Eng. R. 30 (1–2) (2000) 1–54.
[8] V.V. Atuchin, L.D. Pokrovsky, V.G. Kesler, L.I. Isaenko, L.I. Gubenko, Structure and chemistry of LiB_3O_5 LBO) optical surface, J. Ceram. Proc. Res. 4 (2) (2003) 84–87.
[9] V.V. Atuchin, L.D. Pokrovsky, V.G. Kesler, M. N.Yu. Maklakova, N. Yoshimura, T. Ushiyama, K. Matsui, Y. Kamimura, T. Mori, Sasaki, Cesium accumulation at CsB_3O_5 optical surface, Opt. Mater. 23 (2003) 377–383.
[10] V.V. Atuchin, V.G. Kesler, A.E. Kokh, L.D. Pokrovsky, X-ray photoelectron spectroscopy study of β-BaB_2O_4 optical surface, Appl. Surf. Sci. 223 (2004) 352–360.
[11] C. Chen, Z. Lin, Z. Wang, The development of new borate-based UV nonlinear optical crystals, Appl. Phys. B 80 (2005) 1–25.
[12] Valentin Petrov, Masood Ghotbi, Omid Kokabee, Adolfo Esteban-Martin, Frank Noack, Alexander Gaydardzhiev, Ivaylo Nikolov, Pancho Tzankov, Ivan Buchvarov, Kentaro Miyata, Andrzej Majchrowski, Ivan V. Kityk, Fabian Rotermund, Edward Michalski, Majid Ebrahim-Zadeh, Femtosecond nonlinear frequency conversion based on BiB_3O_6, Laser Photon. Rev. 4 (1) (2010) 53–98.
[13] Xin Zhang, Lirong Wang, Shufeng Zhang, Guiling Wang, Sangen Zhao, Yong Zhu, Yicheng Wu, Chuangtian Chen, Optical properties of the vacuum-ultraviolet nonlinear optical crystal—BPO_4, J. Opt. Soc. Am. B 28 (9) (2011) 2236–2239.
[14] N.G. Korobeishchikov, I.V. Nikolaev, V.V. Atuchin, I.P. Prosvirin, A. Tolstogouzov, V. Pelenovich, D.J. Fu, Borate nonlinear optical single crystal surface finishing by argon cluster ion sputtering, Surf. Interfaces 27 (2021) 101520.
[15] P.P. Fedorov, A.E. Kokh, N.G. Kononova, The barium borate β-BaB_2O_4 as a material for nonlinear optics, Uspekhi Khimii 71 (8) (2002) 741–763.
[16] V.P. Solntsev, E.G. Tsvetkov, V.A. Gets, V.D. Antsygin, Growth of a-BaB_2O_4 single crystals from melts at various compositions: comparison of optical properties, J. Cryst. Growth 236 (2002) 290–296.
[17] A.P. Vasilenko, A.V. Kolesnikov, E.M. Trukhanov, N.A. Pylneva, A.M. Yurkin, V.V. Atuchin, X-ray topography study of LiB_3O_5 crystals grown from molybdate flux, J. Phys.: Condens. Matter 15 (2003) 6801–6808.
[18] S. Haussühl, L. Bohatý, P. Becker, Piezoelectric and elastic properties of the nonlinear optical material bismuth triborate, BiB_3O_6, Appl. Phys. A 82 (2006) 495–502.
[19] V.V. Atuchin, V.G. Kesler, A.I. Zaitsev, M.S. Molokeev, A.S. Aleksandrovsky, A.A. Kuzubov, N.Y. Ignatova, Electronic structure of α-SrB_4O_7: experiment and theory, J. Phys.: Condens. Matter 25 (2013) 085503.
[20] Fapeng Yu, Xiulan Duan, Shujun Zhang, Qingming Lu, Xian Zhao, Rare-earth calcium oxyborate piezoelectric crystals $ReCa_4O(BO_3)_3$: Growth and piezoelectric characterizations, Crystals 4 (2014) 241–261.
[21] V.V. Atuchin, B.G. Bazarov, T.A. Gavrilova, V.G. Grossman, M.S. Molokeev, Zh.G. Bazarova, Preparation and structural properties of nonlinear optical borates $K_{2(1-x)}Rb_{2x}Al_2B_2O_7$, 0 < x < 0.75, J. Alloy. Compd. 515 (2012) 119–122.
[22] A.I. Zaitsev, A.S. Aleksandrovsky, A.S. Kozhukhov, L.D. Pokrovsky, V.V. Atuchin, Growth, optical and microstructural properties of PbB_4O_7 plate crystals, Opt. Mater. 37 (2014) 298–301.
[23] Xingxing Jiang, Maxim S. Molokeev, Pifu Gong, Yi Yang, Wei Wang, Shuaihua Wang, Shaofan Wu, Yingxia Wang, Rongjin Huang, Laifeng Li, Yicheng Wu, Xianran Xing, Zheshuai Lin, Near-zero thermal expansion and high ultraviolet transparency in a borate crystal of $Zn_4B_6O_{13}$, Adv. Mater. 28 (2016) 7936–7940.
[24] Miriding Mutailipu, Zhiqing Xie, Xin Su, Min Zhang, Ying Wang, Zhihua Yang, Muhammad Ramzan Saeed Ashraf Janjua, Shilie Pan, Chemical cosubstitution-oriented design of rare-earth borates as potential ultraviolet nonlinear optical materials, J. Am. Chem. Soc. 139 (50) (2017) 18397–18405.
[25] N.A. Nikolaev, Yu.M. Andreev, V.D. Antsygin, T.B. Bekker, D.M. Ezhov, E. Kokh, K.A. Kokh, G.V. Lanskii, A.A. Mamrashev, V.A. Svetlichnyi, Optical properties of β-BBO and potential for THz applications, J. Phys.: Conf. Ser. 951 (2017) 012003.
[26] Zhiqing Xie, Miriding Mutailipu, Guijie He, Guopeng Han, Ying Wang, Zhihua Yang, Min Zhang, Shilie Pan, A series of rare-earth borates $K_7MRE_2B_{15}O_{30}$ (M = Zn, Cd, Pb; RE = Sc, Y, Gd, Lu) with large second harmonic generation responses, Chem. Mater. 30 (7) (2018) 2414–2423.
[27] A.B. Kuznetsov, D.M. Ezhov, K.A. Kokh, N.G. Kononova, V.S. Shevchenko, S.V. Rashchenkoa, E.V. Pestryakov, V.A. Svetlichnyi, I.N. Lapin, A.E. Kokh, Flux growth and optical properties of $K_7CaY_2(B_5O_{10})_3$ nonlinear crystal, Mater. Res. Bull. 107 (2018) 333–338.
[28] Feifei Chen, Xiufeng Cheng, Fapeng Yu, Chunlei Wang, Xian Zhao, Bismuth-based oxyborate piezoelectric crystals: growth and electro-elastic properties, Crystals 9 (2019) 29.
[29] A. Kuznetsov, A. Kokh, N. Kononova, V. Shevchenko, B. Uralbekov, D. Ezhov, V. Svetlichnyi, A. Goreiavcheva, K. Kokh, New scandium borates $R_xLa_ySc_z(BO_3)_4$ (x + y + z = 4, R = Sm, Tb): Synthesis, growth, structure and optical properties, Mater. Res. Bull. 126 (2020) 110850.
[30] A.K. Subanakov, E.V. Kovtunets, B.G. Bazarov, S.G. Dorzhieva, J.G. Bazarova, New double holmium borates: $Rb_3HoB_6O_{12}$ and $Rb_3Ho_2B_3O_9$, Solid State Sci. 105 (2020) 106231.
[31] Zhen Jia, Qindan Zeng, Pifu Gong, Yan Dong, Xiuling Zhang, Bingwei Xin, Zheshuai Lin, Mingjun Xia, Nonlinear-optical crystal $Rb_3YB_6O_{12}$ with condensed B_5O_{10} blocks that exhibits an intriguing structural arrangement and a short ultraviolet absorption edge, Inorg. Chem. 59 (2020) 13029–13033.
[32] Mengen Gao, Hongping Wu, Hongwei Yu, Zhanggui Hu, Jiyang Wang, Yicheng Wu, $BaYOBO_3$: A deep-ultraviolet rare-earth oxy-borate with a large second harmonic generation response, Sci. China Chem. 64 (7) (2021) 1184–1191.
[33] Artem B. Kuznetsov, Konstantin A. Kokh, Nadezda G. Kononova, Vyacheslav S. Shevchenko, Sergey V. Rashchenko, Dmitry M. Ezhov, Ammar Y. Jamous, Asset Bolatov, Bolat Uralbekov, Valery A. Svetlichnyi, Aleksander E. Kokh, Polymorphism in $SmSc_3(BO_3)_4$: Crystal structure, luminescent and SHG properties, J. Alloy. Compd. 851 (2021) 156825.
[34] Feifei Chen, Chao Jiang, Fapeng Yu, Xiufeng Cheng, Xian Zhao, Temperature dependent behaviours of electro-elastic constants for $Bi_2ZnB_2O_7$ piezoelectric crystal, CrystEngComm 23 (2) (2021) 391–396.
[35] Guang Peng, Chensheng Lin, Huixin Fan, Kaichuang Chen, Bingxuan Li, Ge Zhang, Ning Ye, $Be_2(BO_3)(IO_3)$: The first anion-mixed Van der Waals member in $KBe_2BO_3F_2$ family with very strong second harmonic generation response, Angew. Chem. Int. Ed. 60 (32) (2021) 17415–17418.
[36] Mengdi Fan, Guangda Wu, Xinle Wang, Fapeng Yu, Chun Wang, Xian Zhao, Kyropoulos growth and characterization of monoclinic α-$Bi_2B_8O_{15}$ single crystal with a noncentrosymmetric structure, CrystEngComm (2021), https://doi.org/10.1039/d1ce01278a
[37] Sangen Zhao, Guochun Zhang, Jiyong Yao, Yicheng Wu, $K_3YB_6O_{12}$: A new nonlinear optical crystal with a short UV cutoff edge, Mater. Res. Bull. 47 (2012) 3810–3813.

[38] V.V. Atuchin, A.K. Subanakov, A.S. Aleksandrovsky, B.G. Bazarov, J.G. Bazarova, S.G. Dorzhieva, T.A. Gavrilova, A.S. Krylov, M.S. Molokeev, A.S. Oreshonkov, A.M. Pugachev, Yu.L. Tushinova, A.P. Yelisseyev, Exploration of structural, thermal, vibrational and spectroscopic properties of new noncentrosymmetric double borate $Rb_3NdB_6O_{12}$, Adv. Powder Technol. 28 (2017) 1309–1315.
[39] Ji Zhao, Dan Zhao, Ya-Ping Yu, Shan-Xiu Huang, Rui-Juan Zhang, Wei Wei, Zhao Ma, Bao-Zhong Liu, Energy transfer and multicolor tunable emission in single-phase Eu^{3+} doped $K_3TbB_6O_{12}$ phosphors, J. Mater. Sci.: Mater. Electron. 29 (2018) 20199–20205.
[40] V.V. Atuchin, A.K. Subanakov, A.S. Aleksandrovsky, B.G. Bazarov, J.G. Bazarova, T.A. Gavrilova, A.S. Krylov, M.S. Molokeev, A.S. Oreshonkov, S. Yu, Stefanovich, Structural and spectroscopic properties of new noncentrosymmetric self-activated borate $Rb_3EuB_6O_{12}$ with B_5O_{10} units, Mater. Des. 140 (2018) 488–494.
[41] Bing Han, Beibei Liu, Jie Zhang, Yazhou Dai, Hengzhen Shi, Realization of color-tunable emission via energy transfer in novel single-phase $K_3YB_6O_{12}:Bi^{3+}$, Eu^{3+} phosphors, J. Mater. Sci.: Mater. Electron. 30 (19) (2019) 18177–18184.
[42] Bing Han, Beibei Liu, Junping Du, Yazhou Dai, Jie Zhang, Hengzhen Shi, $K_3YB_6O_{12}:Ce^{3+},Tb^{3+}$: A near-ultraviolet-excitable emission-tunable phosphor for white light-emitting diodes, Opt. Laser Technol. 113 (2019) 211–216.
[43] Ying Fu, Zhengzheng Zhang, Feng Zhang, Chao Li, Bitao Liu, Guoqiang Li, Electronic structure, energy transfer mechanism and thermal quenching behavior of $K_3YB_6O_{12}:Dy^{3+}$, Eu^{3+} phosphor, Opt. Mater. 99 (2020) 109519.
[44] Li Yang, Yingpeng Wan, Yanlin Huang, Cuili Chen, Hyo Jin Seo, Development of $YK_3B_6O_{12}$:RE (RE = Eu^{3+}, Tb^{3+}, Ce^{3+}) tricolor phosphors under near-UV light excitation, J. Alloy. Compd. 684 (2016) 40–46.
[45] Li Yang, Yingpeng Wan, Honggen Weng, Yanlin Huang, Cuili Chen, Hyo Jin Seo, Luminescence and color center distributions in $K_3YB_6O_{12}:Ce^{3+}$ phosphor, J. Phys. D: Appl. Phys. 49 (2016) 325303.
[46] Dan Zhao, Fa-Xue Ma, Rui-Juan Zhang, Wei Wei, Juan Yang, Ying-Jie Li, A new rare-earth borate $K_3LuB_6O_{12}$: crystal and electronic structure, and luminescent properties activated by Eu^{3+}, J. Mater. Sci.: Mater. Electron. 28 (1) (2017) 129–136.
[47] Dan Zhao, Cong-Kui Nie, Ye Tian, Bao-Zhong Liu, Yun-Chang Fan, Ji Zhao, A new luminescent host material $K_3GdB_6O_{12}$: synthesis, crystal structure and luminescent properties activated by Sm^{3+}, Z. Krist. 233 (6) (2018) 411–419.
[48] Bing Han, Beibei Liu, Jie Zhang, Yazhou Dai, $K_3YB_6O_{12}:Sm^{3+}$: A novel orange-red emitting phosphor for white light emitting diodes, Optik 179 (2019) 346–350.
[49] Dan Zhao, Fa-Xue Ma, Zhi-Qiang Wu, Lei Zhang, Wei Wei, Juan Yang, Rong-Hua Zhang, Peng-Fei Chen, Shan-Xuan Wu, Synthesis, crystal structure and characterizations of a new red phosphor $K_3EuB_6O_{12}$, Mater. Chem. Phys. 182 (2016) 231–236.
[50] V.V. Atuchin, O.D. Chimitova, S.V. Adichtchev, J.G. Bazarov, T.A. Gavrilova, M.S. Molokeev, N.V. Surovtsev, Zh.G. Bazarova, Synthesis, structural and vibrational properties of microcrystalline β-$RbSm(MoO_4)_2$, Mater. Lett. 106 (2013) 26–29.
[51] V.V. Atuchin, A.S. Aleksandrovsky, M.S. Molokeev, A.S. Krylov, A.S. Oreshonkov, Di Zhou, Structural and spectroscopic properties of self-activated monoclinic molybdate $BaSm_2(MoO_4)_4$, J. Alloy. Compd. 729 (2017) 843–849.
[52] Yu.G. Denisenko, E.I. Sal'nikova, S.A. Basova, M.S. Molokeev, A.S. Krylov, A.S. Aleksandrovsky, A.S. Oreshonkov, V.V. Atuchin, S.S. Volkova, N.A. Khritokhin, O.V. Andreev, Synthesis of samarium oxysulfate $Sm_2O_2SO_4$ in the high-temperature oxidation reaction and its structural, thermal and luminescent properties, Molecules 25 (2020) 1330.
[53] Bruker AXS TOPAS V4: General profile and structure analysis software for powder diffraction data. – User's Manual. Bruker AXS, Karlsruhe, Germany. 2008.
[54] S.K. Kurtz, T.T. Perry, A powder technique for the examination of nonlinear optical materials, J. Appl. Phys. 39 (1968) 3798–3813.
[55] Evgeny V. Alekseev, Olivier Felbinger, Shijun Wu, Thomas Malcherek, Wulf Depmeier, Giuseppe Modolo, Thorsten M. Gesing, Sergey V. Krivovichev, Evgeny V. Suleimanov, Tatiana A. Gavrilova, Lev D. Pokrovsky, Alexey M. Pugachev, Nikolay V. Surovtsev, Victor V. Atuchin, $K[AsW_2O_9]$, the first member of the arsenate–tungsten bronze family: Synthesis, structure, spectroscopic and non-linearoptical properties, J. Solid State Chem. 204 (2013) 59–63.
[56] Dan Zhao, Fa-Xue Ma, Rui-Juan Zhang, Min Huang, Peng-Fei Chen, Rong-Hua Zhang, Wei Wei, Substitution disorder and photoluminescent property of a new rare-earth borate: $K_3TbB_6O_{12}$, Z. Krist. 231 (9) (2016) 525–530.
[57] R.D. Shannon, Revised effective ionic radii and systematic studies of interatomic distances in halides and chalcogenides, Acta Cryst. A 32 (1976) 751–767.
[58] Ernest M. Levin, Robert S. Roth, Jerry B. Martin, Polymorphism of ABO_3-type rare earth borates, Am. Mineral. 46 (1961) 1030–1055.
[59] M. Touboul, $Rb_2(B_4O_5OH)_4(H_2O)_{3.6}$ Univ. de Picardie Jules Verne, Amiens Cedex, France., ICDD Grant-in-Aid (1999).
[60] Sven V. Berger, The crystal structure of boron oxide, Acta Chem. Scand. 7 (1953) P 611-622. Calculated from ICSD using POWD-12++ (1997).
[61] E. Kroumova, M.I. Aroyo, J.M. Perez-Mato, A. Kirov, C. Capillas, S. Ivantchev, H. Wondratschek, Bilbao crystallographic server: useful databases and tools for phase-transition studies, Phase Transit 76 (2003) 155–170.
[62] A.S. Oreshonkov, N.P. Shestakov, M.S. Molokeev, A.S. Aleksandrovsky, I.A. Gudim, V.L. Temerov, S.V. Adichtchev, A.M. Pugachev, I.V. Nemtsev, E.I. Pogoreltsev, Y.G. Denisenko, Monoclinic $SmAl_3(BO_3)_4$: synthesis, structural and spectroscopic properties, Acta Crystallogr. B 76 (2020) 654–660.
[63] A.S. Oreshonkov, E.M. Roginskii, N.P. Shestakov, I.A. Gudim, V.L. Temerov, I.V. Nemtsev, M.S. Molokeev, S.V. Adichtchev, A.M. Pugachev, Y.G. Denisenko, Structural, electronic and vibrational properties of $YAl_3(BO_3)_4$, Materials 13 (2020) 545.
[64] V. Devarajan, E. Gräfe, E. Funck, Raman spectrum and normal coordinate analysis of pentaborate ion (B_5O_{10}) in potassium pentaboratetetrahydrate, Spectrochim. Acta A 32 (1976) 1225–1233.
[65] K. Nakamoto, Infrared and Raman Spectra of Inorganic and Coordination Compounds, 6th ed...,, Wiley,, New York, NY, USA, 2009.